Comparing Sound Radiation from a Loudspeaker with that from a Flexible Spherical Cap on a Rigid Sphere*

RONALD M. AARTS,[1] *AES Fellow,* **AND AUGUSTUS J. E. M. JANSSEN**[2]

(ronald.m.aarts@philips.com)   (a.j.e.m.janssen@tue.nl)

Eindhoven University of Technology, Department of Electrical Engineering, 5600 MB Eindhoven, The Netherlands

It has been suggested by Morse and Ingard that the sound radiation of a loudspeaker in a box is comparable to that of a spherical cap on a rigid sphere. This has been established recently by the present authors, who developed a computation scheme for the forward and inverse calculation of the pressure due to a harmonically excited, flexible cap on a rigid sphere with an axially symmetric velocity distribution. In this paper the comparison is made for other quantities relevant to audio engineers, namely, the baffle-step response, sound power and directivity, and the acoustic center of a radiator.

0 INTRODUCTION

The sound radiation of a loudspeaker is often modeled by assuming the loudspeaker cabinet to be a rigid infinite baffle around a circularly symmetric membrane. Given the velocity distribution on the membrane, the pressure in front of the baffle due to harmonic excitation is then described by Rayleigh's integral [1] or by King's integral [2]. The theory for this model has been firmly established, both analytically and computationally, in many journal papers [3]–[10] and textbooks [11]–[14]. The results thus obtained are in good correspondence with what one obtains when the loudspeaker is modeled as a finite-extent boxlike cabinet with a circular, vibrating membrane [15], [16]. This statement should, however, be restricted to the region in front of the loudspeaker and not too far from the axis. The validity of the infinite-baffle model becomes questionable, or even nonsensical, in the side regions or behind the loudspeaker [12, p. 181].

It has been suggested by Morse and Ingard [11, sec. 7.2] that using a sphere with a membrane on a spherical cap as a simplified model of a loudspeaker whose cabinet has roughly the same width, height, and depth, produces results comparable to the true loudspeaker. Such a cap model can be used to predict the polar behavior of a loudspeaker cabinet. Pressure calculations for true

loudspeakers can normally only be done by using advanced numerical techniques [15], [16]. In the case of the spherical-cap model the pressure can be computed as the solution of Helmholtz equation with spherical boundary conditions in the form of series involving the products of spherical harmonics and spherical Hankel functions [17, ch. 11.3], [18, ch. III, sec. 6], [11, ch. 7], [19, ch. 19–21], using coefficients that are determined from the boundary conditions at the sphere, including the flexible cap. In [20] there is a discussion on how the polar-cap model for a sphere of radius $R \rightarrow \infty$ agrees with the model that uses the flat piston in an infinite baffle. When the cap aperture angle θ_0 approaches π, the solution becomes that of a simple pulsating sphere. Hence the polar-cap solution subsumes the solutions of the two classic radiation problems. This very same issue, for the case of a piston, has been addressed by Rogers and Williams [21]. In [22] the spherical-cap model has been used to describe sound radiation from a horn.

In [23] the authors of the present paper make a detailed comparison, on the level of polar plots, of the pressure (SPL) due to a true loudspeaker and the pressure computed using the spherical-cap model. The standard computation scheme for this model has been modified in [23] in the interest of solving the inverse problem of estimating the velocity distribution on the membrane from measured pressure data around the sphere. To accommodate the stability of the solution of this inverse problem, an efficient parametrization of velocity profiles vanishing outside the cap in terms of expansion coefficients with respect to orthogonal functions on the cap is used. This leads to a more complicated computation scheme than the standard one, with the advantage that it can be used in both forward and reverse directions. The emphasis in the present paper is on comparing acoustical quantities that can be obtained from the

---

[1] Also with Philips Research Laboratories, 5656 AE Eindhoven, The Netherlands.

[2] Also with Eindhoven University of Technology, EURAN-DOM.

spherical-cap model by forward computation, and so the more complicated scheme in [23] is not needed. Hence the standard scheme is used in the present paper.

The quantities considered in this paper for comparing the results from a true loudspeaker with those produced by using the spherical cap are:

- Baffle step response
- Sound power and directivity
- Acoustic center.

In Section 1 the geometry and a detailed overview of the basic formulas and some results from [23] are given. Section 2 compares the baffle-step response computed using the spherical-cap model with the one obtained from the loudspeaker. In Section 3 the same is done for the sound power and directivity, while in Section 4 the acoustic center is considered. In Section 5 the conclusions and outlook for further work are presented.

1 GEOMETRY AND BASIC FORMULAS

Assume an axisymmetric velocity profile $V(\theta)$ in the normal direction on a spherical cap S_0, given in spherical coordinates as

$$S_0 = \{(r, \theta, \varphi) | r = R, \, 0 \le \theta \le \theta_0, \, 0 \le \varphi \le 2\pi\} \quad (1)$$

with R being the radius of the sphere with its center at the origin and θ_0 the aperture angle of the cap measured from the center. The half-line $\theta = 0$ is identified with the positive z direction in the Cartesian coordinate system. See Fig. 1 for the geometry and notations used. It is assumed that V vanishes outside S_0. Furthermore, as is commonly the case in loudspeaker applications, the cap moves parallel to the z axis according to the component

$$W(\theta) = V(\theta)\cos \theta, \quad (2)$$
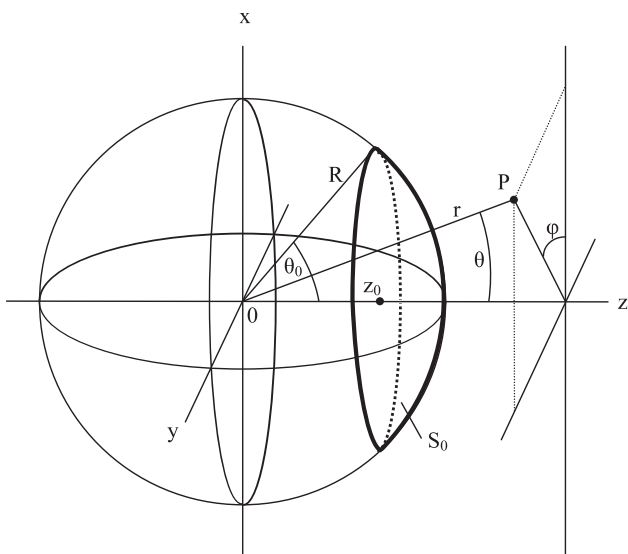
of V in the z direction. The average of this z component

over the cap,

$$\frac{1}{A_{S_0}} \iint_{S_0} W(\theta)\sin \theta \, d\theta \, d\varphi, \qquad A_{S_0} = 4\pi R^2 \sin^2\left(\frac{\theta_0}{2}\right) \quad (3)$$

with A_{S_0} being the area of the cap, is denoted by w_0. The time-independent part $p(r, \theta)$ of the pressure due to a harmonic excitation of the flexible membrane with the z component W of the velocity distribution is given by

$$p(r, \theta) = -i\rho_0 c \sum_{n=0}^{\infty} W_n P_n(\cos \theta) \frac{h_n^{(2)}(kr)}{h_n^{(2)'}(kR)}. \quad (4)$$

See [11, ch. 7] or [19, ch. 19]. Here ρ_0 is the density of the medium, c is the speed of sound in the medium, $k = \omega/c$ is the wavenumber, with ω the radial frequency of the applied excitation, and $r \ge R$, $0 \le \theta \le \pi$. (The azimuthal variable φ is absent because of the assumption of axisymmetrical profiles.) Furthermore P_n is the Legendre polynomial of degree n [24]. The coefficients W_n are given by

$$W_n = \left(n + \frac{1}{2}\right) \int_0^\pi W(\theta) P_n(\cos \theta)\sin \theta \, d\theta,$$
$$n = 0, 1, ... \quad (5)$$

and $h_n^{(2)}$ and $h_n^{(2)'}$ are the spherical Hankel function and its derivative of order $n = 0, 1, \ldots$ [24, ch. 10].

The case where $W = w_0$ is constant on the cap has been treated in [18, pt. III, sec. 6], [11, p. 343], and [19, sec. 20.5], with the result that

$$W_n = \frac{1}{2} w_0 [P_{n-1}(\cos \theta_0) - P_{n+1}(\cos \theta_0)]. \quad (6)$$

The pressure p is then obtained by inserting these W_n into the right-hand side of Eq. (4). Similarly the case where $V = v_0$ is constant on S_0 has been treated in [19, sec. 20.6], with the result that

$$W_n = \frac{1}{2} v_0 \left\{ \frac{n+1}{2n+3} [P_n(\cos \theta_0) - P_{n+2}(\cos \theta_0)] \right.$$
$$\left. + \frac{n}{2n-1} [P_{n-2}(\cos \theta_0) - P_n(\cos \theta_0)] \right\}. \quad (7)$$

In Eqs. (6) and (7) the definition $P_{-n-1} = P_n$, $n = 0, 1, \ldots$, has been used to deal with the case $n = 0$ in Eq. (6) and the cases $n = 0, 1$ in Eq. (7). In [23, eq. (20)] a formula for the expansion coefficients W_n in terms of the expansion coefficients of the profile W with respect to orthogonal functions on the cap is given. This formula is instrumental in solving the inverse problem of estimating W from pressure data measured around the sphere. However, for the present goal, which can be achieved by forward computation, this is not needed.

Fig. 2, taken from [23, fig. 2], shows the resemblance between the polar plots of a real driver in a rectangular cabinet [Fig. 2(a)], a rigid piston in an infinite baffle [Fig. 2(b)], and a rigid spherical cap in a rigid sphere [Fig. 2(c)] using Eqs. (4) and (7). The driver (vifa MG10SD09–08, $a = 32$ mm) was mounted in the square side of a rectangular

Fig. 1. Geometry and notations.

cabinet with dimensions of 130 by 130 by 186 mm and measured on a turntable in an anechoic room at 1-m distance.

The area A_{S_0} of the spherical cap is given by Eq. (3). If this area is chosen to be equal to the area of the flat piston (a disk with radius a), then it follows that

$$a = 2R \sin\left(\frac{\theta_0}{2}\right). \tag{8}$$

The parameters used for Fig. 2, namely, $a = 32$ mm, $\theta_0 =$ $\pi/8$, and $R = 82$ mm, are such that the areas of the piston and the cap are equal, while the sphere and the cabinet have comparable volumes (2.3 and 3.1 l, respectively). If R were chosen such that the sphere and the cabinet have equal volume, the polar plot corresponding to the spherical-cap model would be hardly different from the one in Fig. 2(c), with deviations of about 1 dB or less (see [23, fig. 2(c),(d)]). Apparently the actual value of the volume is of modest influence. It is hard to give strict bounds to deviations from the actual size, but as a rule of thumb one can choose the volume of the sphere to be the
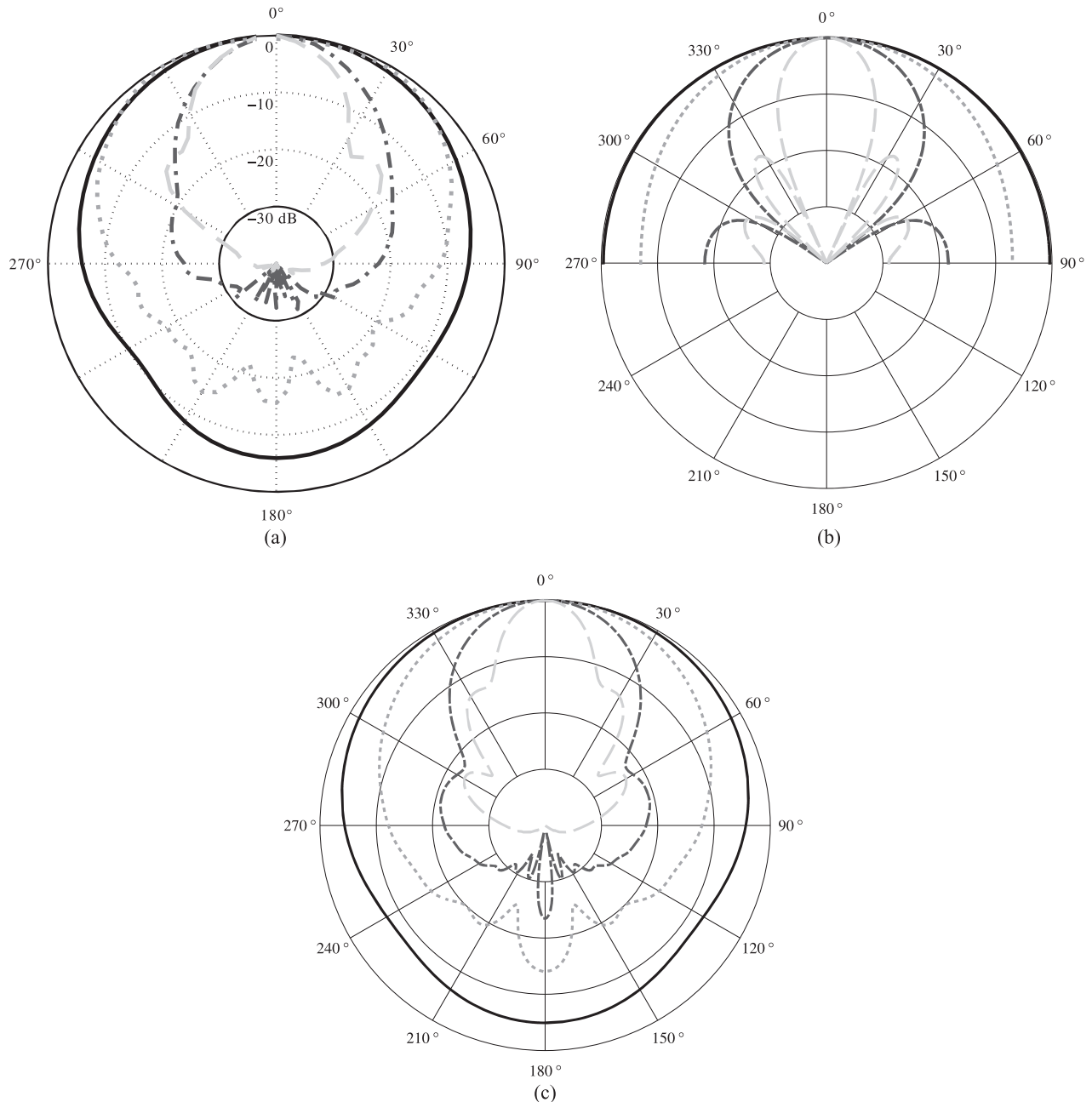

Fig. 2. Polar plots of SPL (10 dB/div). —$f = 1$ kHz; $\cdots f = 4$ kHz; $-\cdot -f = 8$ kHz; $---f = 16$ kHz; $c = 340$ m/s, $a = 32$ mm; ka $= 0.591, 2.365, 4.731, 9.462$. All curves are normalized such that SPL is 0 dB at $\theta = 0$. (a) Loudspeaker ($a = 32$ mm, measuring distance $r = 1$ m) in rectangular cabinet. (b) Rigid piston ($a = 32$ mm) in infinite baffle. (c) Rigid spherical cap ($\theta_0 = \pi/8$, sphere radius $R = 82$ mm, $r = 1$ m, corresponding to $kR = 1.5154, 6.0614, 12.1229, 24.2457$). Constant velocity $V = v_0 = 1$ m/s. Parameters a, R, and θ_0 are such that areas of piston and cap are equal.

same as that of the real cabinet, and the area of the cap to be the same as that of the driver. To gain more insight into this matter we keep R fixed and change the cap area by changing the aperture θ_0. To illustrate that the influence can be significant, polar plots are shown in Fig. 3 for constant $V = v_0 = 1$ m/s, using Eqs. (4) and (7). Fig. 3 clearly shows that when the aperture angle θ_0 is increased until, say, $\theta_0 = \pi/2$, the radiation becomes more directive.

In the limit case $\theta_0 = \pi$ there is only one nonzero W_n in Eqs. (6) and (7), that is, $W_n = \delta_{0n}$ for constant W and $W_n = \delta_{1n}$ for constant V, respectively (δ being the Kronecker

delta). In the case of constant W this is a nondirective pulsating sphere. In the case of constant V we have

$$p(r, \theta) = -\mathrm{i}\rho_0 c v_0 \cos\theta \, \frac{h_1^{(2)}(kr)}{h_1^{(2)\prime}(kR)}. \tag{9}$$

The latter case is discussed in [13, sec. 4.2] as the transversely oscillating rigid sphere. It is readily seen that $p(r, \theta)/p(r, 0) = \cos\theta$, as plotted in Fig. 4. Finally consider the case of a simple source with a δ mass b at the point $(0, 0, z = R)$. This can be obtained by taking $W(\theta) = w_0 = b/A_{S_0}$, $0 \leq \theta \leq \theta_0$, and letting θ_0 decrease to 0. Since $P_n(1) = 1$ for all n, Eq. (5) gives $W_n = (2n + 1)b$ for
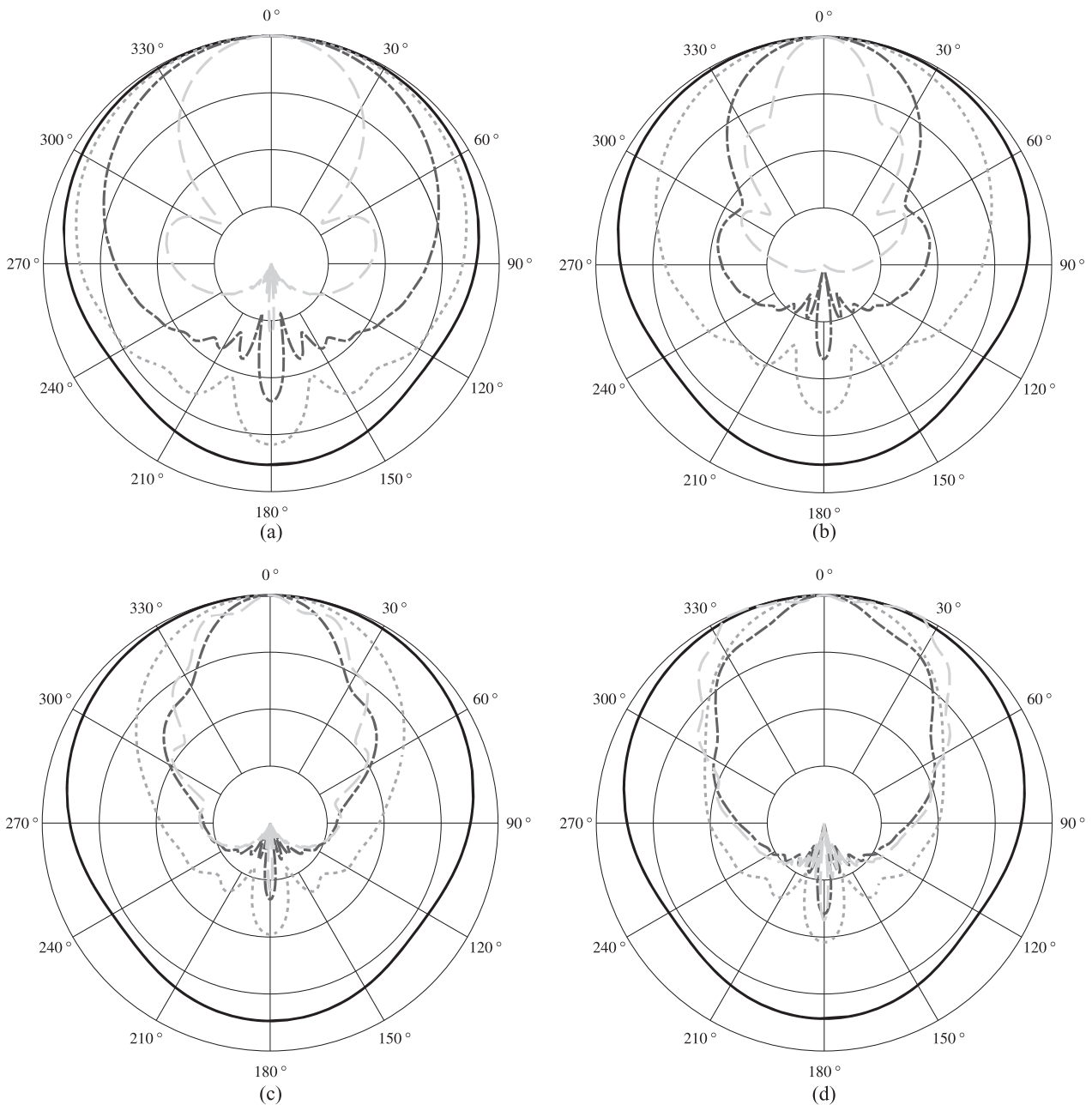

Fig. 3. Polar plots of SPL (10 dB/div). —$f = 1$ kHz; $\cdots f = 4$ kHz; $-\cdot-f = 8$ kHz; $---f = 16$ kHz. Rigid spherical cap for various apertures θ_0. Sphere radius $R = 82$ mm; $r = 1$ m; constant velocity $V = v_0 = 1$ m/s. All curves are normalized such that SPL = 0 dB at $\theta = 0$. (a) $\theta_0 = \pi/16$; (b) $\theta_0 = 2\pi/16$; (c) $\theta_0 = 3\pi/16$; (d) $\theta_0 = 4\pi/16$.

all n as θ_0 goes to 0, and there results

$$p(r, \theta) = -i\rho_0 cb \sum_{n=0}^{\infty} (2n+1) P_n(\cos\theta) \frac{h_n^{(2)}(kr)}{h_n^{(2)'}(kR)}. \quad (10)$$

This case is illustrated in [23, fig. 3], from which it is apparent that the responses at $\theta = 0$ and $\theta = \pi$ are of the same order of magnitude, especially at low frequencies. This is discussed further in Section 3.2 in connection with the acoustic center.

2 COMPARISON OF BAFFLE-STEP RESPONSES

At low frequencies the baffle of a loudspeaker is small compared to its wavelength, and it radiates due to diffraction effects in the full space (4π field). At those low frequencies the radiator does not benefit from the baffle in terms of gain. At high frequencies the loudspeaker benefits from the baffle, which yields a gain of 6 dB. This transition is the well-known baffle step. The center frequency of this transition depends on the size of the baffle. Olson [25] has documented this for 12 different loudspeaker enclosures, including the sphere, cylinder, and rectangular parallelepiped. All those 12 enclosures share the common feature of increasing gain by about 6 dB when the frequency is increased from low to high. The exact shape of this step depends on the particular enclosure. For spheres the transition is smoothest, while for other shapes undulations occur, in particular for cabinets with sharp-edged boundaries. In Fig. 5(a) the baffle step is shown for a polar cap ($\theta_0 = \pi/8$, constant velocity $V = v_0 = 1$ m/s) on a sphere of radius $R = 0.082$ m using Eqs. (4) and (7), for different observation angles θ. Compare the curves in Fig. 5(a) with the measurements using the experimental loudspeaker [Fig. 5(b)], discussed in Section 1, and that of a rigid piston in an infinite baffle [Fig. 5(c)]. Using [12]–[14],

$$\frac{p_i(\theta)}{p_i(\theta = 0)} = \frac{J_1[ka\sin(\theta)]}{[ka\sin(\theta)]} \quad (11)$$

for the normalized pressure. It appears that there is a good resemblance between the measured frequency response of the experimental loudspeaker and the polar cap model. The undulations, for example, for $\theta = 3\pi/9$ (dashed curve), at 7.4, 10, and 13.4 kHz correspond well. Although these undulations are often attributed to the nonrigid cone movement of the driver itself, our illustrations show that it is mainly a diffraction effect. Furthermore it can be observed that even on axis ($\theta = 0$) there is a gradual decrease in SPL at frequencies above about 10 kHz. It can be shown from the asymptotics of the spherical Hankel functions that for $\theta = 0$, $k \to \infty$, and $r \gg R$, the sound pressure $p(r, \theta)$ decays at least as $O(k^{-1/3})$. This is in contrast to a flat piston in an infinite baffle [Fig. 5(c)]. There the on-axis pressure does not decay, and the baffle step is absent. This is discussed

further at the end of Section 3.2. Although it is highly speculative, and should be validated for different drivers and cabinets, one might expect that the ratio of the pressure of the cap using Eqs. (4) and (7) to that of the piston in an infinite baffle using Eq. (11) can assist in interpreting published loudspeaker response curves that are measured under standardized (infinite-baffle) conditions. For typical loudspeakers at low frequencies the loss is theoretically 6 dB, but is counteracted by room placement. A range of 3–6 dB is usually allowed. At sufficiently high frequencies the piston does not benefit from the baffle because it is highly directional. Finally the tests were done using a high-quality 3.5-inch loudspeaker. In such a unit the first cone breakup mode usually occurs around 10 kHz. However, the present case does not exhibit a clear breakup mode because it is very well damped. This was verified by means of a PolyTec PSV-300-H scanning vibrometer with an OFV-056 laser head.

3 COMPARISON OF POWER AND DIRECTIVITY

3.1 Sound Power

The sound power is meaningful in various respects. First it is used in efficiency calculations, which we do not consider here. Second it is important with regard to sound radiation. Different loudspeakers may share a common, rather flat on-axis SPL response, while their off-axis responses differ considerably. Therefore we consider the power response important. We restrict ourselves to axisymmetric drivers and we do not discuss horn loudspeakers. The power is defined as the intensity $pv*$
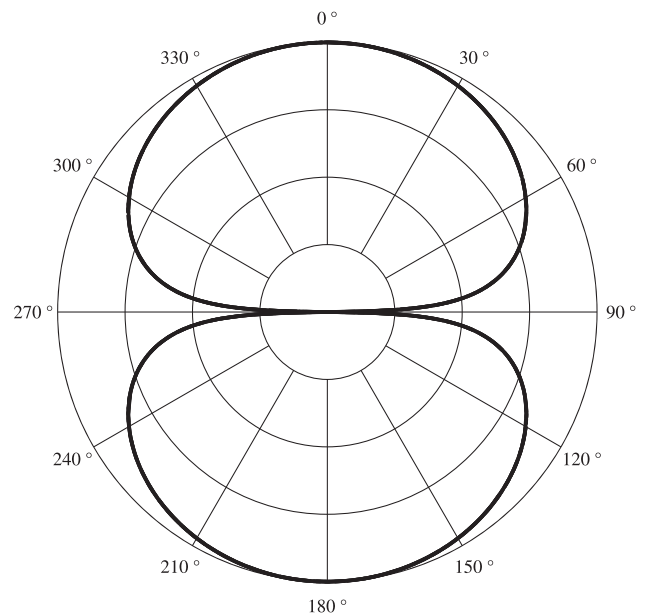

Fig. 4. Polar plot for sphere ($\theta_0 = \pi$) moving with constant velocity $V = v_0 = 1$ m/s in z direction. $W_1 = 1$; $W_n = 0$ for all $n \neq 1$.
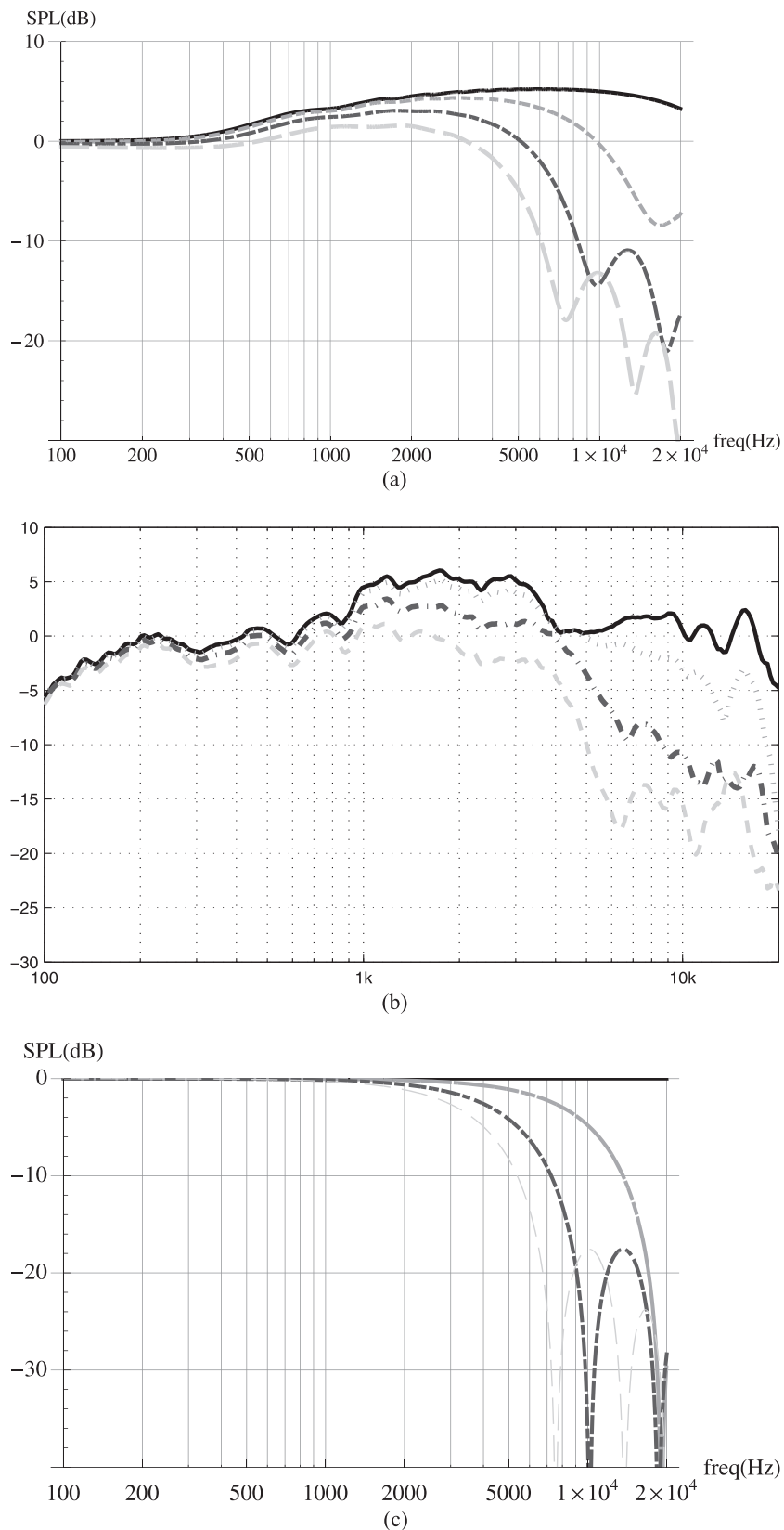
Fig. 5. Frequency responses. — $\theta = 0$; $\cdots$ $\theta = \pi/9$; $-\cdot-$ $\theta = 2\pi/9$; $---$ $\theta = 3\pi/9$. (a) Baffle step of polar cap ($\theta_0 = \pi/8$) on sphere of radius $R = 82$ mm, $r = 1$ m; constant velocity $V = v_0 = 1$ m/s. All curves are normalized such that SPL $= 0$ dB at 100 Hz. (b) Frequency response of driver [same as Fig. 2(a), $a = 32$ mm] mounted in square side of a rectangular cabinet with dimensions $130 \times 130 \times 186$ mm. Loudspeaker was measured in an anechoic room at 1-m distance. On-axis response was normalized to 0 dB at 200 Hz, other curves were normalized by same amount. (c) Response of rigid piston ($a = 32$ mm) in infinite baffle in the far field. All curves are normalized such that SPL $= 0$ dB at 100 Hz.

integrated over the sphere S_r of radius $r \geq R$,

$$P = \int_{S_r} pv^* \, dS_r \tag{12}$$

where p and v are pressure and velocity at an arbitrary point on the sphere S_r. Using Eq. (4) for the pressure and

$$v = \frac{-1}{ik\rho_0 c} \frac{\partial p}{\partial \underline{n}} \tag{13}$$

we get

$$v(r, \theta, \varphi) = \sum_{n=0}^{\infty} W_n P_n(\cos \theta) \frac{h_n^{(2)'}(kr)}{h_n^{(2)'}(kR)}. \tag{14}$$

By the orthogonality of the Legendre polynomials it follows that

$$P = \int_{S_r} pv^* \, dS_r = 2\pi \int_0^{\pi} p(r, \theta) v^*(r, \theta) r^2 \sin \theta \, d\theta$$

$$= -i\rho_0 c \sum_{n=0}^{\infty} \frac{|W_n|^2}{n + \frac{1}{2}} \frac{2\pi r^2 h_n^{(2)}(kr)[h_n^{(2)'}(kr)]^*}{\left| h_n^{(2)'}(kR) \right|^2}. \tag{15}$$

Using [24, eq. 10.1.6],

$$\mathcal{W}\{j_n(z), y_n(z)\} = j_n(z) y_n'(z) - j_n'(z) y_n(z) = \frac{1}{z^2} \tag{16}$$

where $\mathcal{W}$ denotes the Wronskian, we get

$$\Re[P] = \frac{2\pi \rho_0 c}{k^2} \sum_{n=0}^{\infty} \frac{|W_n|^2}{\left(n + \frac{1}{2}\right) \left| h_n^{(2)'}(kR) \right|^2}. \tag{17}$$

Note that Eq. (17) has been derived without using any (near-field or far-field) approximation. The real part of the acoustic power is independent of r, which is in accordance with the conservation of power law. For low frequencies Eq. (17) is approximated as

$$\Re[P] = 4\pi \rho_0 c W_0^2 k^2 R^4. \tag{18}$$

To illustrate Eq. (17), the normalized power $\Re[P]/2\pi \rho_0 c v_0^2 R^2$ is plotted in Fig. 6, where a cap with various apertures is moving with constant velocity $V = v_0 = 1$ m/s [using Eqs. (7) and (17)].

Next we compare the calculated power with the power measured in a reverberation room using the experimental loudspeaker discussed in Section 1. Here we assumed the pole cap moving not with constant velocity but with constant acceleration ($V' = ikcV$), corresponding to a frequency-independent current of constant amplitude through the loudspeaker. Fig. 7 shows plots of the calculated power for a rigid spherical cap moving with constant acceleration and at various apertures, together with the power obtained from the measured loudspeaker. It appears that the calculated power for $\theta_0 = \pi/8$ and the power from the measured loudspeaker are quite similar while there was no special effort made to obtain a best fit. A slightly larger aperture

than the "round" value $\theta_0 = \pi/8$, which we use in many examples in this paper, would have resulted in a better fit. The low-frequency behavior of Fig. 7 follows directly from multiplying Eq. (18) with $1/(kc)^2$ because of the constant acceleration of the cap.

3.2 Directivity

The far-field pressure can be calculated by substituting the asymptotic value [24, ch. 10]

$$h_n^{(2)}(kr) \approx i^{n+1} \frac{e^{-ikr}}{kr} \tag{19}$$

in Eq. (4), which leads to

$$p(r, \theta) \approx \rho_0 c \frac{e^{-ikr}}{kr} \sum_{n=0}^{\infty} \frac{i^n W_n}{h_n^{(2)'}(kR)} P_n(\cos \theta). \tag{20}$$

In Kinsler et al. [12, sec. 8.9] the far-field relation is written as

$$p(r, \theta, \varphi) = p_{ax}(r) H(\theta, \varphi) \tag{21}$$

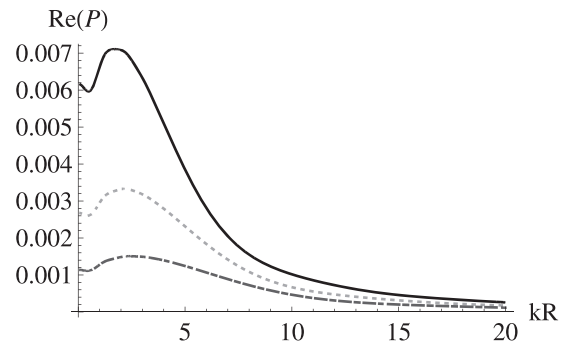in which $p_{ax}(r)$ is the pressure at $\theta = 0$, and $H(\theta, \varphi)$ is

Fig. 6. Power $\Re[P]/2\pi\rho_0 c v_0^2 R^2$ of rigid spherical cap moving with constant velocity $V = v_0 = 1$ m/s for various apertures. — $\theta_0 = 5\pi/32$; $\cdots$ $\theta_0 = \pi/8$; $-\cdot-$ $\theta_0 = \pi/10$. Sphere radius $R = 82$ mm.
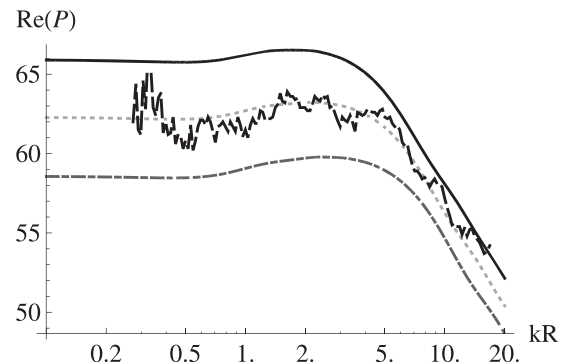

Fig. 7. Power $\Re[P]c/2\pi\rho_0 a_0^2 R^4$ [dB] versus kR (log axis) of rigid spherical cap moving with constant acceleration $V' = ikcV$ for various apertures. — $\theta_0 = 5\pi/32$; $\cdots$ $\theta_0 = \pi/8$; $-\cdot-$ $\theta_0 = \pi/10$; irregular curve—Power from measured loudspeaker. Sphere radius $R = 82$ mm. Logarithmic horizontal axis runs from $kR = 0.1$ to 20, corresponding to a frequency range of 66 Hz to 13.2 kHz.

dimensionless with $H(0, 0) = 1$. Since there is no φ dependence, we delete it. This leads to

$$p_{ax}(r) = \rho_0 c \frac{e^{-ikr}}{kr} \sum_{n=0}^{\infty} \frac{i^n W_n}{h_n^{(2)'}(kR)} \tag{22}$$

and

$$H(\theta) = \frac{p(r, \theta)}{p_{ax}(r)} = \frac{\displaystyle\sum_{n=0}^{\infty} \frac{i^n W_n}{h_n^{(2)'}(kR)} P_n(\cos\theta)}{\displaystyle\sum_{n=0}^{\infty} \frac{i^n W_n}{h_n^{(2)'}(kR)}} . \tag{23}$$

The total radiated power Π in the far field follows from Eq. (12) and the far-field relation $v = p/\rho_0 c$ as

$$\Pi = \int_{S_r} \frac{1}{\rho_0 c} |p|^2 \, dS_r$$
$$= \frac{1}{\rho_0 c} |p_{ax}(r)|^2 r^2 \int_0^{2\pi} \int_0^{\pi} |H(\theta)|^2 \sin\theta \, d\theta \, d\varphi. \tag{24}$$

For a simple (nondirective) source at the origin to yield the same acoustical power on S_r, the pressure p_s should satisfy

$$\Pi = \frac{1}{\rho_0 c} 4\pi r^2 |p_s(r)|^2. \tag{25}$$

Therefore the directivity defined as

$$D = \frac{|p_{ax}(r)|^2}{|p_s(r)|^2} \tag{26}$$

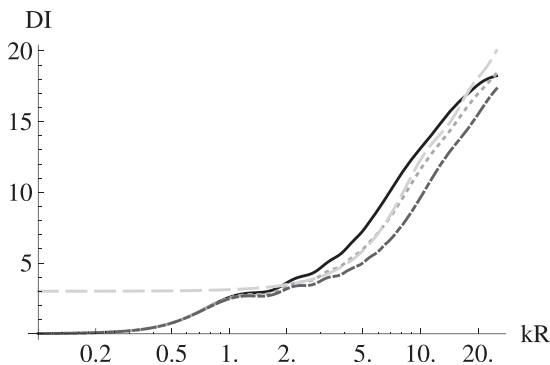follows from Eqs. (23)–(25), using the orthogonality of

DI

Fig. 8. Directivity index DI $= 10 \log_{10} D$ [dB] versus kR (log axis) of rigid spherical cap for various apertures. — $\theta_0 = 5\pi/32$; $\cdots$ $\theta_0 = \pi/8$; $-\cdot-$ $\theta_0 = \pi/10$. Constant velocity V; sphere radius $R = 82$ mm. $---$ curve starting at 3 dB is directivity for rigid piston in an infinite baffle, using Eq. (28). Logarithmic horizontal axis runs from $kR = 0.1$ to 25, corresponding to a frequency range of 66 Hz to 16.5 kHz.

the Legendre polynomials, as

$$D = \left[2 \left| \sum_{n=0}^{\infty} \frac{i^{n+1} W_n}{h_n^{(2)'}(kR)} \right|^2 \right] \left[\sum_{n=0}^{\infty} \frac{|W_n|^2}{\left(n + \frac{1}{2}\right) \left| h_n^{(2)'}(kR) \right|^2} \right]^{-1} . \tag{27}$$

The directivity index DI $= 10 \log_{10} D$ [dB] versus kR is plotted in Fig. 8 for a cap moving with constant velocity V. For comparison the directivity

$$D_{rp} = \frac{(ka)^2}{1 - J_1(2ka)/ka} \tag{28}$$

of a rigid piston in an infinite baffle [12] is plotted in Fig. 8 by the dashed curve starting at 3 dB (with $ka = kR/2.5$, so that the $\pi/8$ cap and piston have the same area). At low frequencies the directivity D_{rp} is 3 dB because the piston is radiating in the 2π field while the caps are radiating in the 4π field. At higher frequencies the curve almost coincides with the dotted curve, which corresponds to the $\theta_0 = \pi/8$ cap.

Now consider the case where $kR \to \infty$. Then using $h_n^{(2)'}(kR) \approx i^n e^{-ikR}/kR$, it follows that D is approximated by

$$D \approx \frac{2 \left| \displaystyle\sum_{n=0}^{\infty} W_n \right|^2}{\displaystyle\sum_{n=0}^{\infty} \frac{|W_n|^2}{n + \frac{1}{2}}} = \frac{2|W(\theta = 0)|^2}{\displaystyle\int_0^{\pi} |W(\theta)|^2 \sin\theta \, d\theta} \tag{29}$$

or, in words, by the ratio of $|W(\theta = 0)|^2$ to the average value of $|W(\theta)|^2$ over the sphere. Eqs. (27) and (29) show that the directivity—which is a typical far-field acoustical quantity—is fully determined in a simple manner by the velocity profile of the pole cap, which can be easily derived from measurements, such as with a laser Doppler meter. This procedure is not discussed here. A similar result was obtained for a flexible radiator in an infinite flat baffle [10]. In the flat-baffle case the directivity increases with $(ka)^2$. For the cap case there is indeed an initial increase with $(kR)^2$, but at very high frequencies there is a decrease in directivity. In most cases these high frequencies are beyond the audio range, but may be of importance for ultrasonics. The deviation of the $(kR)^2$ behavior appears in Fig. 8 for θ_0 as low as $5\pi/32$ (solid curve). This effect may seem counterintuitive or even nonphysical. However, the on-axis ($\theta = 0$) pressure decreases for high frequencies as well (see Fig. 5). This will decrease the numerator on the right-hand side of Eq. (26). This effect does not occur with a piston in an infinite baffle, which has a constant, nondecreasing on-axis sound pressure, but a narrowing beamwidth.

4 ACOUSTIC CENTER

The acoustic center of a reciprocal transducer can be defined as the point from which spherical waves seem to be diverging when the transducer is acting as a source. There are, however, additional definitions. See [26] for an overview and discussion. This concept is used mainly for microphones. Recently the acoustic center was discussed [27], [28] for normal sealed-box loudspeakers as a particular point that acts as the origin of the low-frequency radiation of the loudspeaker. At low frequencies the radiation from such a loudspeaker becomes simpler as the wavelength of the sound becomes larger relative to the enclosure dimensions, and the system behaves externally as a simple source (point source). The difference between the origin and the true acoustic center is denoted by Δ. If $p(r, 0)$ and $p(r, \pi)$ are the sound pressure in front and at the back of the source, then Δ follows from

$$\frac{|p(r, 0)|}{r + \Delta} = \frac{|p(r, \pi)|}{r - \Delta} \tag{30}$$

as

$$\Delta = r \frac{|q| - 1}{|q| + 1} \tag{31}$$

where

$$q = \frac{p(r, 0)}{p(r, \pi)}. \tag{32}$$

The pole-cap model is used to calculate the function q via Eq. (4); see Fig. 9.

Subsequently this model is used to compute the acoustic center with Eq. (31). Assume that $kR \ll 1$ and $R/r \ll 1$, and also that W_n is real with W_n of at most the same order of magnitude as W_0. Then two terms of the series in Eq. (4) are sufficient, and using $P_n(1) = 1$ and $P_n(-1) = (-1)^n$, q can be written as

$$q \approx \left[W_0 \frac{h_0^{(2)}(kr)}{h_0^{(2)'}(kR)} + W_1 \frac{h_1^{(2)}(kr)}{h_1^{(2)'}(kR)} \right]$$

$$\times \left[W_0 \frac{h_0^{(2)}(kr)}{h_0^{(2)'}(kR)} - W_1 \frac{h_1^{(2)}(kr)}{h_1^{(2)'}(kR)} \right]^{-1}. \tag{33}$$

Because $kR \ll 1$, the small argument approximation of the spherical Hankel functions

$$h_0^{(2)'}(z) \approx \frac{-i}{z^2}, \qquad h_1^{(2)'}(z) \approx \frac{-2i}{z^3} \tag{34}$$

can be used, and together with the identity

$$\frac{h_1^{(2)}(kr)}{h_0^{(2)}(kr)} = \frac{1}{kr}(1 + ikr) \tag{35}$$

we get

$$q \approx \left[1 + \frac{W_1}{2W_0}(1 + ikr)\frac{R}{r} \right] \left[1 - \frac{W_1}{2W_0}(1 + ikr)\frac{R}{r} \right]^{-1}. \tag{36}$$

By our assumptions we have

$$\left| \frac{W_1}{2W_0}(1 + ikr)\frac{R}{r} \right| \ll 1$$

and so

$$q \approx 1 + \frac{W_1}{W_0}\frac{R}{r}(1 + ikr). \tag{37}$$

Finally assuming that

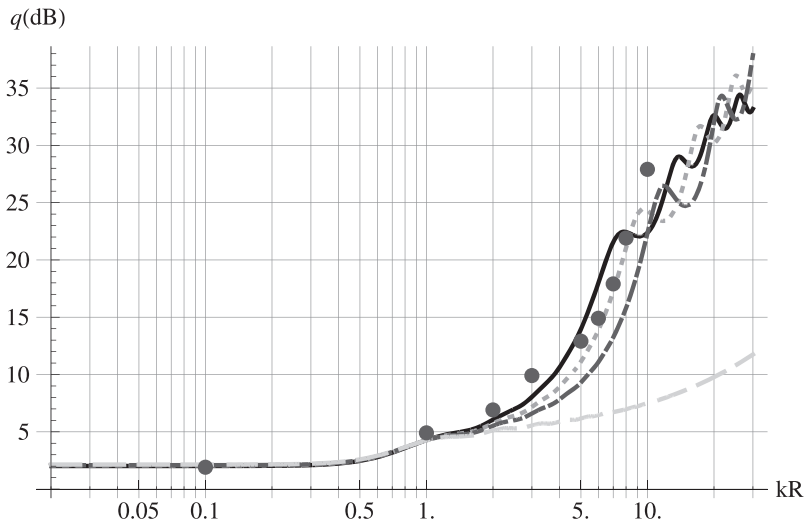$$(kr)^2 \ll 2\left| \frac{W_0}{W_1} \right|\frac{r}{R},$$

Fig. 9. Function $20 \log_{10}|q|$ [dB] versus kR (log axis) [Eq. (32)] of rigid spherical cap for various apertures. — $\theta_0 = 5\pi/32$; $\cdots$ $\theta_0 = \pi/8$; — · — $\theta_0 = \pi/10$; – – – simple source on sphere using Eq. (10). Constant velocity V, all at $r = 1$ m; sphere radius $R = 82$ mm. Solid circles—real driver [same as Fig. 2(a); $a = 32$ mm] mounted in square side of a rectangular cabinet. Logarithmic horizontal axis runs from $kR = 0.02$ to 30, corresponding to a frequency range of 13 Hz to 19.8 kHz.

there holds

$$|q| \approx 1 + \frac{W_1}{W_0}\frac{R}{r} \tag{38}$$

and if $W_1 R / W_0 r \ll 1$ there holds

$$\varphi_q = \arg q \approx \arctan \frac{W_1}{W_0}\frac{\omega R}{c} \tag{39}$$

where it has been used that W_1/W_0 is real and $k = \omega/c$. Substitution of Eq. (38) into Eq. (31) results in

$$\Delta \approx \frac{RW_1}{2W_0}. \tag{40}$$

Note that this result is real, independent of k and r, and only mild assumptions were used. The delay between the front and the back of the source is equal to $\tau = d\varphi_q/d\omega$. Using Eqs. (39) and (40), and assuming $kR \ll W_0/W_1$ we get

$$\tau \approx \frac{2\Delta}{c}. \tag{41}$$

For the case where W is constant the W_n follow from Eq. (6), resulting in

$$\Delta \approx \frac{3}{4}R(1 + \cos \theta_0). \tag{42}$$

If $\theta_0 = \pi$ and W is constant, the radiator is a pulsating sphere and, according to Eq. (42), has its acoustical center at the origin. For the case V is constant the W_n follow from Eq. (7), resulting in

$$\Delta \approx R\left(\cos \theta_0 + \frac{1}{1 + \cos \theta_0}\right). \tag{43}$$

If $\theta_0 = \pi$ and V is constant, the notion of acoustical center does not make sense because of the notches in the polar plot at low frequencies (see Fig. 4). The absolute error in the approximation of Δ/R by Eq. (43) (for $f = 1$ Hz, $R = 82$ mm, $r = 100$ m, and $0 \leq \theta_0 \leq \pi/2$) is $< 5 \times 10^{-7}$. Fig. 9 shows that for a cap moving with constant velocity V the low-frequency asymptote is flat to about $kR = 0.4$, corresponding to 264 Hz. Hence the approximation of Δ/R by Eq. (43) is rather accurate up to this frequency. The
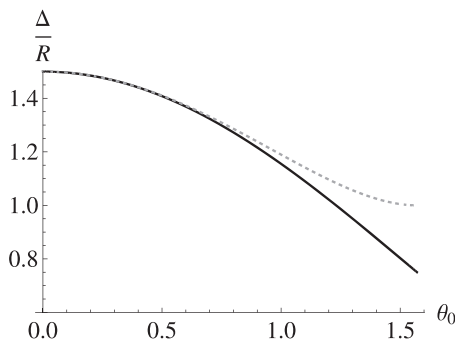

Fig. 10. Relative acoustic center difference Δ/R versus θ_0. — using Eq. (42) for W constant; $\cdots$ using Eq. (43) for $V = v_0 = 1$ m/s constant.

relative acoustic center difference Δ/R versus θ_0 is plotted in Fig. 10 for constant W and V, using Eqs. (42) and (43). Note that $\Delta/R = 3/2$ for $\theta_0 = 0$ in both cases and that V and W are constant. This agrees with what would be given by the simple source on a sphere [see Eq. (10)]. We have $W_0 = 1$ and $W_1 = 3$, and by Eq. (40) we obtain $\Delta/R = 3/2$. For low frequencies this is also shown in [26, fig. 3, eqs. 18–19]. Further it appears that for modest apertures, say, $\theta_0 \leq 0.5$, the difference between the right-hand sides of Eqs. (42) and (43) is very small, on the order of θ_0^4. From this we may conclude that—at low frequencies ($kR \leq 0.4$)—the acoustic center for a loudspeaker lies about 0–0.5R in front of the loudspeaker, where R is the radius in the case of a spherical cabinet, or some other dimensional measure of the cabinet. At higher frequencies the acoustic center shifts further away from the loudspeaker. For example, between $kR = 1$ (660 Hz) and $kR = 2$ (1.32 kHz) q is about 5 dB (see Fig. 9), corresponding to $\Delta = 3.4R = 280$ mm [using Eq. (31)].

The polar response $|p(r, \theta)/p(r, 0)|$ at low frequencies can be computed in a similar way as q in Eq. (36). The minus sign in the denominator on the right-hand side of Eq. (36) is due to $P_1(\cos \pi) = -1$. Using now $P_1(\cos \theta) = \cos \theta$ and interchanging the numerator and denominator of Eq. (36) yields

$$\frac{p(r, \theta)}{p(r, 0)} \approx \left[1 + \frac{W_1}{2W_0}(1 + ikr)\frac{R}{r}\cos \theta\right]$$
$$\times \left[1 + \frac{W_1}{2W_0}(1 + ikr)\frac{R}{r}\right]^{-1}. \tag{44}$$

Assuming that

$$(kr)^2 \ll 2\left|\frac{W_0}{W_1}\right|\frac{r}{R},$$

Eq. (44) can be approximated by

$$\left|\frac{p(r, \theta)}{p(r, 0)}\right| \approx 1 + (\cos \theta - 1)\frac{W_1}{2W_0}\frac{R}{r}. \tag{45}$$

Eq. (45) clearly shows that the deviation from omnidirectional radiation is proportional to the ratios $W_1/2W_0$ and R/r while it is independent of frequency for low frequencies. For fixed $W_1/2W_0$ and R/r the polar pattern is not truly omnidirectional at low frequencies. This is because the acoustic center does not coincide with the origin in general.

5 CONCLUSIONS AND OUTLOOK

The polar plot of a rigid spherical cap on a rigid sphere has been shown to be quite similar to that of a real loudspeaker (see Fig. 2) and is useful in the full 4π field. It thus outperforms the more conventional model in which the loudspeaker is modeled as a rigid piston in an infinite baffle. The cap model can be used to predict, besides polar plots, various other acoustical quantities of a loudspeaker. These quantities include sound pressure, baffle-step response, sound power, directivity, and the

acoustic center. The baffle-step response of the model is rather similar to that of a loudspeaker (see Fig. 5). The sound power predicted by the model is very similar to that of a loudspeaker measured in a reverberation room (see Fig. 7). The directivity D given by the model is approximated as the ratio of $|W(\theta=0)|^2$ to the average value of $|W(\theta)|^2$ over the sphere [see Eq. (29)]. The ratio of the sound pressure in front and at the back of the loudspeaker, which is associated with the acoustic center, is for a loudspeaker very similar to that given by the model (see Fig. 9). At low frequencies the acoustic center for a loudspeaker lies about 0–0.5 times the sphere radius in front of the loudspeaker (see Fig. 10). At higher frequencies the acoustic center shifts further away from the loudspeaker. All results are obtained using one loudspeaker only. The value of this model for other drivers in other cabinets should be tested in order to derive bounds for the applicability of the model. This work remains to be done in the future.

6 ACKNOWLEDGMENT

7 REFERENCES

[1] J. W. S. Rayleigh, *The Theory of Sound*, vol. 2, (1896; reprinted by Dover, New York, 1945).

[2] L. V. King, "On the Acoustic Radiation Field of the Piezo-Electric Oscillator and the Effect of Viscosity on Transmission," *Can. J. Res.*, vol. 11, pp. 135–155 (1934).

[3] M. Greenspan, "Piston Radiator: Some Extensions of the Theory," *J. Acoust. Soc. Am.*, vol. 65, pp. 608–621 (1979 March).

[4] G. R. Harris, "Review of Transient Field Theory for a Baffled Planar Piston," *J. Acoust. Soc. Am.*, vol. 70, pp. 10–20 (1981 July).

[5] T. Hasegawa, N. Inoue, and K. Matsuzawa, "A New Rigorous Expansion for the Velocity Potential of a Circular Piston Source," *J. Acoust. Soc. Am.*, vol. 74, pp. 1044–1047 (1983 Sept.).

[6] D. A. Hutchins, H. D. Mair, P. A. Puhach, and A. J. Osei, "Continuous-Wave Pressure Fields of Ultrasonic Transducers," *J. Acoust. Soc. Am.*, vol. 80, pp. 1–12 (1986 July).

[7] R. C. Wittmann, and A. D. Yaghjian, "Spherical-Wave Expansions of Piston-Radiator Fields," *J. Acoust. Soc. Am.*, vol. 90, pp. 1647–1655 (1991 Sept.).

[8] T. J. Mellow, "On the Sound Field of a Resilient Disk in an Infinite Baffle," *J. Acoust. Soc. Am.*, vol. 120, pp. 90–101 (2006 July).

[9] R. M. Aarts and A. J. E. M. Janssen, "On-Axis and Far-Field Sound Radiation from Resilient Flat and Dome-Shaped Radiators," *J. Acoust. Soc. Am.*, vol. 125, pp. 1444–1455 (2009 March).

[10] R. M. Aarts and A. J. E. M. Janssen, "Sound Radiation Quantities Arising from a Resilient Circular Radiator," *J. Acoust. Soc. Am.*, vol. 126, pp. 1776–1787 (2009 Oct.).

[11] P. M. Morse and K. U. Ingard, *Theoretical Acoustics* (McGraw-Hill, New York, 1968).

[12] L. E. Kinsler, A. R. Frey, A. B. Coppens, and J. V. Sanders, *Fundamentals of Acoustics* (Wiley, New York, 1982).

[13] A. D. Pierce, *Acoustics—An Introduction to Its Physical Principles and Applications* (Acoustical Society of America through the American Institute of Physics, 1989).

[14] D. T. Blackstock, *Fundamentals of Physical Acoustics* (Wiley, New York, 2000).

[15] H. Suzuki and J. Tichy, "Sound Radiation from Convex and Concave Domes in an Infinite Baffle," *J. Acoust. Soc. Am.*, vol. 69, pp. 41–49 (1981 Jan.).

[16] H. Suzuki and J. Tichy, "Radiation and Diffraction Effects of Convex and Concave Domes," *J. Audio Eng. Soc.*, vol. 29, pp. 873–881 (1981 Dec.).

[17] P. M. Morse and H. Feshbach, *Methods of Theoretical Physics* (McGraw-Hill, New York, 1953).

[18] H. Stenzel and O. Brosze, *Guide to Computation of Sound Phenomena* (published in German as *Leitfaden zur Berechnung von Schallvorgängen*), 2nd ed. (Springer, Berlin, 1958).

[19] E. Skudrzyk, *The Foundations of Acoustics* (Springer, New York, 1971; reprinted by Acoustical Society of America, 2008).

[20] R. New, R. I. Becker, and P. Wilhelmij, "A Limiting Form for the Nearfield of the Baffled Piston," *J. Acoust. Soc. Am.*, vol. 70, pp. 1518–1526 (1981 Nov.).

[21] P. H. Rogers and A. O. Williams, Jr., "Acoustic Field of Circular Plane Piston in Limits of Short Wavelength or Large Radius," *J. Acoust. Soc. Am.*, vol. 52, pp. 865–870 (1972 Sept.).

[22] T. Hélie and X. Rodet, "Radiation of a Pulsating Portion of a Sphere: Application to Horn Radiation," *Acta Acustica/Acustica*, vol. 89, pp. 565–577 (2003 July/Aug.).

[23] R. M. Aarts and A. J. E. M. Janssen, "Sound Radiation from a Resilient Spherical Cap on a Rigid Sphere," *J. Acoust. Soc. Am.*, vol. 127, pp. 2262–2273 (2010 Apr.).

[24] M. Abramowitz and I. A. Stegun, *Handbook of Mathematical Functions* (Dover, New York, 1972).

[25] H. F. Olson, "Direct Radiator Loudspeaker Enclosures," *J. Audio Eng. Soc.*, vol. 17, pp. 22–29 (1969 Jan.).

[26] F. Jacobsen, S. Barrera Figueroa, and K. Rasmussen, "A Note on the Concept of Acoustic Center," *J. Acoust. Soc. Am.*, vol. 115, pp. 1468–1473 (2004 Apr.).

[27] J. Vanderkooy, "The Acoustic Center: A New Concept for Loudspeakers at Low Frequencies," presented at the 121st Convention of the Audio Engineering

Society, *J. Audio Eng. Soc. (Abstracts)*, vol. 54, p. 1261 (2006 Dec.), convention paper 6912.

[28] J. Vanderkooy, "The Low-Frequency Acoustic Center: Measurement, Theory, and Application,"

presented at the 128th Convention of the Audio Engineering Society, *(Abstracts)* www.aes.org/events/128/128thWrapUp.pdf, (2010 May), convention paper 7992.

THE AUTHORS

R. M. Aarts

A. J. E. M. Janssen

Ronald M. Aarts was born in Amsterdam, The Netherlands in 1956. He received a B.Sc. degree in electrical engineering in 1977 and a Ph.D. degree in physics from Delft University of Technology in 1995.

He joined the Optics Group at Philips Research Laboratories, Eindhoven, The Netherlands, in 1977 and initially investigated servos and signal processing for use in both Video Long Play players and Compact Disc players. In 1984 he joined the Acoustics Group at Philips Research Laboratories and worked on the development of CAD tools and signal processing for loudspeaker systems. In 1994 he became a member of the Digital Signal Processing (DSP) Group at Philips Research Laboratories and has led research projects on the improvement of sound reproduction by exploiting DSP and psychoacoustical phenomena. In 2003 he became a Research Fellow at the Philips Research Laboratories and extended his interests in engineering to medicine and biology. He is part-time full professor at the Eindhoven University of Technology.

Dr. Aarts has published a large number of papers and reports and holds over 150 first patent application filings, including over 35 granted US patents in the aforementioned fields. He has served on a number of organizing committees and as chairman for various international conventions. He is a Fellow of the IEEE, a Silver Medal recipient, Fellow, and past governor of the Audio Engineering Society, a member of the Dutch Acoustical

Society, the Acoustical Society of America, the Dutch Society for Biophysics and Biomedical Engineering, and the Dutch Society for Sleep and Wake Research.

●

Augustus J. E. M. Janssen received engineering and Ph.D. degrees in mathematics from the Eindhoven University of Technology, The Netherlands, in 1976 and 1979, respectively. From 1979 to 1981 he was a Bateman Research Instructor in the Mathematics Department of the California Institute of Technology. From 1981 until 2010 he worked with Philips Research Laboratories, Eindhoven, where his principal responsibility was to provide high-level mathematical service and consultancy in mathematical analysis. He is currently affiliated with the Departments of Mathematics (EURANDOM) and of Electrical Engineering at the Eindhoven University of Technology, where he provides consultancy in mathematical analysis.

Dr. Janssen has published over 180 papers in the fields of Fourier analysis, signal analysis, time–frequency analysis, electron microscopy, optical diffraction theory, and queueing theory. His current interests include the application of techniques from the theory of optical aberrations to the characterization of acoustical radiators. He is a Fellow of the IEEE.